

# Scalable quantum computing stabilised by optical tweezers on an ion crystal

Yu-Ching Shen and Guin-Dar Lin

Center for Quantum Science and Engineering and Department of Physics, National Taiwan University, Taipei 10617, Taiwan

E-mail: guindar.lin@gmail.com

October 2019

**Abstract.** As it has been demonstrated that trapped ion systems have unmatched long-lived quantum-bit (qubit) coherence and can support high-fidelity quantum manipulations, how to scale up the system size becomes an inevitable task for practical purposes. In this work, we theoretically analyse the physical limitation of scalability with a trapped ion array, and propose a feasible scheme of architecture that in principle allows an arbitrary number of ion qubits, for which the overhead only scales linearly with the system size. This scheme relies on the combined ideas of a trap architecture of tunable size, stabilisation of an ion crystal by optical tweezers, and continuous sympathetic cooling without touching the stored information. We demonstrate that illumination of optical tweezers modifies the motional spectrum by effectively pinning the ions, lifting the frequencies of the motional ground modes. By doing so, we make the structure of the array less vulnerable from thermal excitations, and suppress the position fluctuations to insure faithful gate operations. Finally, we also explore the local behaviour of cooling when a sub-array is isolated by optical tweezers from other parts of the crystal.

## 1. Introduction

As some prototype quantum computing (QC) resources have emerged in the commercial market for recent years, there have been more and more user experiences and exploding interest in quantum technologies and algorithms that aim to demonstrate its supremacy over any classical means. In addition to the solid-state realisation based on superconducting circuits, trapped ion systems remain one of the most promising alternative platforms. Up to present, they retain the record ( $\sim 99.9\%$ ) of highest fidelities of quantum state and gate manipulation [1, 2, 3], and the largest size of engineered qubit entanglement [4, 5]. The latest benchmark test report released by IonQ Inc. has shown very competitive results [6]. Further, such systems offer a perfect bottom-up approach to investigate many-body correlation and quantum simulation [7, 8, 9] as well as other perspectives in the study of atomic clocks, non-classical motional states, and phonon lasers of growing interest very recently.

A typical ion trap, as known as the Paul trap, is constructed by time-varying radiofrequency (RF) electric field, which confines and aligns ions in a linear structure. In QC, each ion serves as a quantum-bit (qubit) as the information is encoded in two of the atomic states. The qubit degrees of freedom are protected from ions' motion unless the coupling between motion and qubit states are turned on by applying state-dependent forces. During the quantum gate processing, the collective motion is used as the quantum bus. The entanglement between motion and qubit states is crucial for gate operations, but needs to be removed when the operation is completed. Any residual entanglement introduces computational errors and heat for subsequent operations. The most commonly used scheme nowadays is the Mølmer-Sørensen-Milburn gate [10, 11], which utilizes bi-chromatic interference to eliminate temperature dependence so can be operated at higher temperatures. It is further shown that, by operating the transverse modes [12], a faithful gate can be accomplished requiring only the Doppler cooling [13].

Though ion systems excel other platforms in many ways such as long-lived atomic coherence, perfectly identical qubits, strong laser-mediated Coulomb interaction, and deterministic control engineered entanglement, the major challenge is its scalability. There have been several scalable proposals including ion shuttling [14, 15, 16, 17], quantum network [17, 18, 19], and arrays of microtraps [20, 21], which, however, introduces new issues of hardware fabrication (shuttling, microtraps), movement control (shuttling), slow processing speed (shuttling), and probabilistic and lossy quantum interfacing (quantum network). The 1D geometry of a Paul trapped ion array is the most straightforward, but seems very difficult to scale up. Nevertheless, it is still worth investigating the fundamental reasons of such limitation in 1D for it might provide informative insights in more complicated structures. Here, we discuss the scalable issues in the following: (1) Architecture issue – Adding more ions requires building a larger trap. The desired architecture must be scalable with single qubit addressability. To avoid nearby ion cross-talking, the ions' spacing  $d_0$  must be kept a few microns (in this paper, we take  $d_0 = 10 \mu\text{m}$ ) to allow a focused Gaussian beam of width approximately half of the spacing. Further, it is beneficial to have gate controlling parameters universal along the crystal, without considering the actual location where gates are performed as long as the distance of target qubits (gate distance) is fixed. Thus, the ideal geometry must be uniform [13]. (2) Array stability and cooling issue – For a very large linear ion array, the bottom of the trap is usually flat in order for the ions distributed uniformly. In this case, the lowest frequencies of the longitudinal motion vanish. The ground mode, for instance, corresponds to collective macroscopic translation, and may cause qubit ions to move off sites and make them hardly addressable. Also, these motional states heat up easily due to divergent phonon numbers, thus jeopardizing the stability of the array structure. (3) Gate design issue – In a large array, it fails to realize a two-qubit gate in the adiabatic regime due to the unresolvable collective motional spectrum. Fortunately, gate operation is still possible by taking into account multi-modes that contribute to local motional degrees of freedom of involved ions. This suggests usage of fast gate operation such that the local motion will not 'spread' out over the whole system. Two

major such protocols are the push gate scheme based on pulsed lasers [23, 24, 25, 26] and the pulse shaping scheme based on continuous-wave lasers [12, 13, 27, 28, 29]. These fast gates have been shown to have very high fidelity but demand strong laser power.

In this manuscript, we aim at resolving the architecture and cooling issues by proposing a scalable trapping scheme for a large linear ion crystal, stabilised by optical tweezers. Optical tweezers are dipole traps formed by off-resonant Gaussian beams that can be focused to about a few microns of beam width so are able to illuminate individual ions. Typically, dipole trapping forces are much weaker than Coulomb forces between charged particles so may not be very useful for confining ions. But for a large array, the Coulomb forces from each other are cancelled in the mechanical equilibrium positions of ions. The relevant frequency scale is then determined by the residual Coulomb interaction, i.e., the next order of the Coulomb interaction while the ions are perturbatively displaced from the equilibrium. This frequency scale characterising the momentum exchange between adjacent ions is given by  $\omega_0 \equiv \sqrt{e^2/(md_0^3)}$  (discussed below), where  $e$  and  $m$  are the charge and mass, respectively, of an ion. With  $\omega_0$  typically ranging from a few hundreds of kilohertz to megahertz, we will show how the application of optical tweezers of frequency about the same order of magnitude modifies the motional spectrum to improve stability of the crystal and help with the cooling problems.

This manuscript is organized as follows: In Sec. 2, we propose a scalable architecture where a large ion crystal can be constructed. We analyse the associated motional spectrum and discuss the stabilisation made by introducing the optical tweezers. In Sec. 3, we demonstrate high-fidelity gates based on transverse modes of the uniform array, focusing on the locality and the translation symmetry of the controlling parameters. We also discuss the major sources of gate errors due to thermal noises. Sec. 4 investigates the sympathetic cooling performance on the ion crystal, where we show that the position fluctuations are suppressed in the presence of optical tweezers under cooling. Further, in Sec. 5 we look at the local dynamics of a sub-array when it is exclusively cooled while isolated by optical tweezers, demonstrating a remarkable feature of locality that is important for parallel manipulation and cooling. Finally, we conclude this work by Sec. 6.

## 2. Scalable architecture

A typical Paul trap is shown in Fig. 1(a). Here, we take the planar trap for example [30], but our following analysis applies to other realisations. To contain a uniform large 1D array, the trapping potential must have a flat bottom with both ends terminated by two walls, resembling a pair of ‘bookends’ as depicted by Fig. 1(b). The trap size (separation between two bookends) should be adjustable in order for holding more ions. Fig. 1(a) demonstrates a practical implementation, where two parallel RF wires (in blue) provide the transverse confinement that supports the ion array above by a separation  $h$ ; along the axial direction paves a segmental structure of electrodes with each piece separated

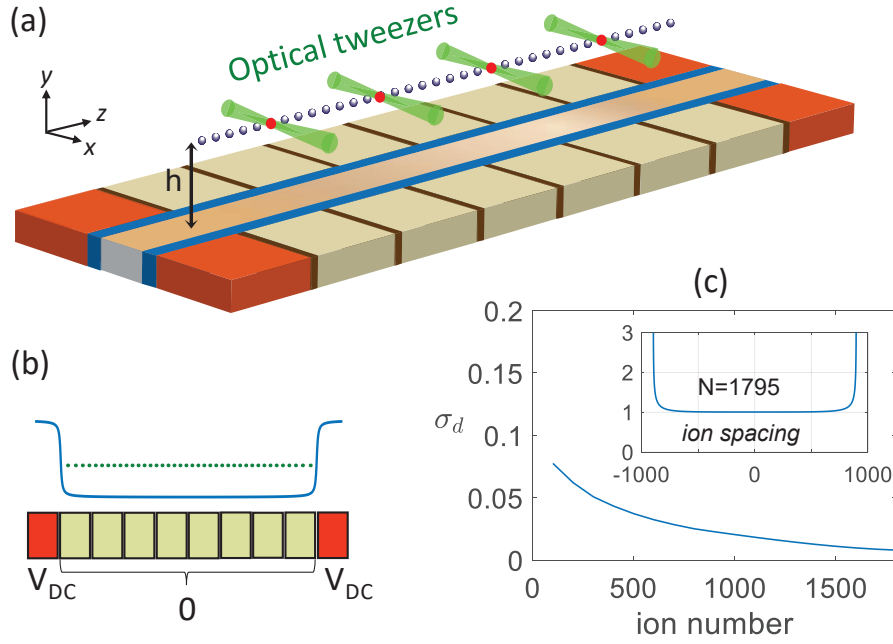


**Figure 1.** (a) Scalable ion trap architecture for a planar realisation [30] for quantum computing with a series of optical tweezers applied on regularly distributed ions over the crystal. (b) The surface DC electrodes build a ‘bookend’-like potential whose size can be adjusted according to the system size. (c) Uniformity characterised by standard deviations  $\sigma_d$  of ion spacing for various system sizes by keeping the mean spacing equal to  $d_0$ . Here, we take  $L = 100qd_0$  for  $q = 1, 2, \dots, 20$  as the distance between two bookend walls and  $V_{\text{DC}} = 0.1$  V (see text). The mean and standard deviation of spacing are taken from only the 80% ions in the middle of the crystal. (Inset) The spacing distribution for an ion crystal of length  $N = 1795$  in units of  $d_0$ .

by thin isolating layers such that each piece can be applied a different DC voltage. Most of the pieces are set to the ground except by the trap edges the potential is lifted for global confinement. Here we describe the bookend potential landscape in Fig. 1(b) by the simplified model:

$$U(z) = \begin{cases} \frac{eV_{\text{DC}}}{\pi} \left( \tan^{-1} \frac{h}{z + \frac{L}{2}} - \tan^{-1} \frac{h}{z - \frac{L}{2}} \right) & \text{for } |z| \leq \frac{L}{2} \\ \frac{eV_{\text{DC}}}{\pi} \left( \tan^{-1} \frac{h}{z + \frac{L}{2}} - \tan^{-1} \frac{h}{z - \frac{L}{2}} + \pi \right) & \text{for } |z| > \frac{L}{2} \end{cases} \quad (1)$$

where the voltage applied to the edge electrodes is  $V_{\text{DC}} > 0$ , and the bookend-to-bookend distance is  $L$ . By taking  $h = 30 \mu\text{m}$  and  $V_{\text{DC}} = 0.1$  V, we calculate the classical equilibrium positions of the ions. When the ion number gets large ( $> 10^2$ ), the array can be made rather equally spaced if we only take the middle 80% of the array into account. The uniformity characterised by the standard deviation is shown in Fig. 1(c), where we observe that the uniformity is less than 4% for  $N > 500$ . The actual spacing distribution is also plotted for  $N = 1795$  and  $L = 2000d_0$  with  $d_0 = 10 \mu\text{m}$ . Note that the unequal spacing near the edges is inevitable since those ions experience non-uniform

forces from rest of the array and the bookend potential. But they can be excluded from computing tasks due to lack of homogeneity.

As any part of an array might expose to environmental noises and collisions, a larger system is more vulnerable for being more likely to be disturbed. These disturbances contribute to heating in a sense, and can be dealt with by cooling techniques. The associated fundamental difficulty is that the lowest motional frequency  $\omega_L$  vanishes as  $N \rightarrow \infty$ , so the position fluctuations and the phonon number  $\bar{n} \sim k_B T / (\hbar \omega_L)$  diverge for any given finite temperature. To circumvent this problem, we propose to apply optical tweezers to alter the motional spectrum. Here, a characteristic frequency scale is determined by the next order of the Coulomb interaction, that is, the residual term  $e^2/d_0^3 \equiv m\omega_0^2$ , which gives  $\omega_0 \equiv \sqrt{e^2/(md_0^3)}$  that accounts for the momentum exchange between adjacent ions. Typically,  $\omega_0$  is about  $0.1 \sim 1$  MHz, such conditions allow dipole traps such as optical tweezers of frequency on the same order of magnitude to make significant differences. For an ion array sitting in the equilibrium, the interaction can be expressed under the harmonic approximation as  $\sum_{i,j} A_{ij}^\xi x_i^\xi x_j^\xi$  with the coupling matrix elements  $A_{ii}^\xi = \nu_{\xi,i}^2 + \nu_{\xi,i}^{\text{ot}2} + \sum_{l=1, l \neq i}^N c_\xi / |u_i - u_l|^3$  and  $A_{ij}^\xi = -c_\xi / |u_i - u_j|^3$  for  $i \neq j$ , where  $\xi = x, y$  denote two transverse directions, and  $\xi = z$  the longitudinal direction;  $c_x = c_y = -1$ , and  $c_z = 2$ ;  $u_i$  is the equilibrium  $z$  position of the  $i$ th ion in units of  $d_0$ . Also,  $\nu_{\xi,i} = \omega_{\xi,i} / \omega_0$  and  $\nu_{\xi,i}^{\text{ot}} = \omega_{\xi,i}^{\text{ot}} / \omega_0$  are dimensionless frequencies. For  $^{171}\text{Yb}^+$  ions, we have  $\omega_0 = 2\pi \times 143$  kHz for  $d_0 = 10$   $\mu\text{m}$ , which is taken to be the exemplary system throughout this manuscript. In addition, the RF transverse confinement frequency  $\omega_{x,i} = \omega_{y,i} = 2\pi \times 5$  MHz is the same for all ions. The longitudinal one is given by the second-order derivative of the potential (1)  $\nu_{z,i}^2(z) = (\omega_0^2 m)^{-1} \partial^2 U / \partial z^2$  evaluated at  $z = u_i d_0$ . The frequency  $\omega_{\xi,i}^{\text{ot}}$  is provided by the optical tweezers experienced by the  $i$ th ion ( $\omega_{\xi,i}^{\text{ot}} = 0$  means no tweezers). Here we also assume that the optical tweezer beams, if present, are incident along the  $x$  direction so that  $\omega_{y,i}^{\text{ot}} = \omega_{z,i}^{\text{ot}} > 0$ . Along the  $x$  direction of incidence, even though there is a trapping effect due to spatial variation of a focused Gaussian beam, we take  $\omega_{x,i}^{\text{ot}} \approx 0$  because it is usually much smaller than the RF one  $\omega_{x,i}$ .

To see how optical tweezers help stabilise a large ion crystal, we first consider the arrangement shown in Fig.1(a). Here, a series of optical tweezers are regularly distributed shining on ions with a spatial repetition period  $P = 10$  sites over the system. Hereafter, the ions that are illuminated by optical tweezers are called ‘tweezered’ ions in this manuscript. The application of optical tweezers amounts to introducing separators partitioning the whole ion crystal into ‘cells’. An array of cells of the same size is thus constructed by inserting these optical tweezers with each cell containing  $P - 1$  ions. In Fig.2(a), we show that, for  $P = 10$  and  $N \sim 10^3$ , the lowest longitudinal frequency  $\omega_L$  can be raised by one to two orders of magnitude by simply applying tweezers of frequency up to 500 kHz. With tweezer strength larger than 5 MHz, the frequency profile appears to converge to the case of infinite tweezer strength, meaning that these tweezered ions are effectively pinned in space. Fig.1(b) shows the lowest frequency against the period  $P$  of the tweezer distribution, where we find  $\omega_L / \omega_0 \approx 3.36 P^{-0.77}$ . This

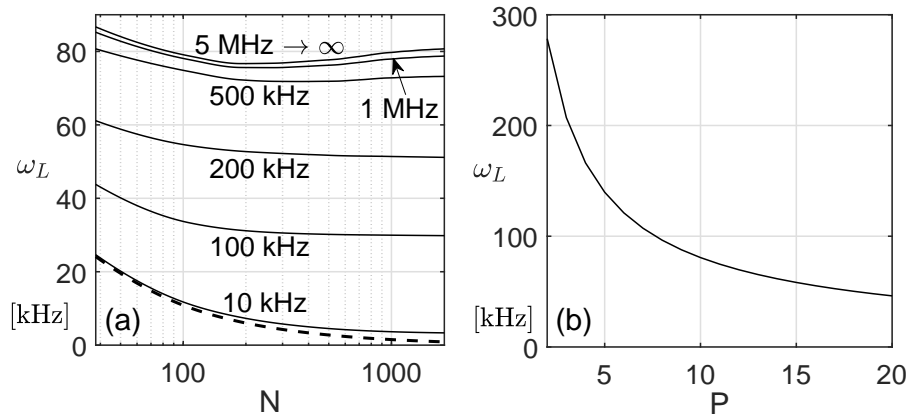


**Figure 2.** (a) The lowest longitudinal frequency in kHz with various optical tweezer strength for different system sizes  $N$ . The optical tweezers are applied every  $P = 10$  ion sites. For comparison, the dashed curve represents to tweezer-free cases. Note that for the tweezer strength larger than  $2\pi \times 1$  MHz, the systems start to display similar motional spectral distribution. This means that the ‘tweezered ions’ can be effectively treated completely frozen. (b) Lowest frequency in kHz as a function of repetition period  $P$  for  $N = 1795$  and  $L = 2000d_0$ . In all cases, we take  $V_{DC} = 0.1$  V and  $h = 30$   $\mu\text{m}$ .

frequency scale is comparable to that of a single cell, implying that the corresponding modes are determined dominantly by local degrees. The emerging localization of motion is a remarkable feature as the tweezer frequency becomes sufficiently strong, or multiple tweezered ions are bundled to be treated as a separator. This point will be discussed in the context of cooling in Sec.5. On the other hand, since optical tweezers are off-resonant dipole traps, in principle they do not evoke population transitions. But AC Stark dephasing may still occur and degrade the coherence. Though it can be somewhat calibrated, it should be avoided to store quantum information in tweezered ions. Fortunately, we hold the flexibility to turn optical tweezers on and off at any time. That is, tweezered ions are recyclable.

### 3. Quantum gate and fidelity

Quantum gates are implemented by coupling internal and motional states, exchanging quantum information via common collective phonon modes. On a large ion array, the motional spectrum becomes rather complicated and hardly resolvable. Therefore, a working quantum gate needs to involve multiple motional modes at the same time. Superposition of these modes in fact contributes to local motion of the target ions and their neighbouring ones. Given that the ion crystal is uniform, the local degrees associated with such a quantum gate must have translation symmetry, i.e., the control parameters are universal no matter where the gate is implemented as long as the distance of the two target qubits is given. Quantum gates over larger distance demand stronger laser power. Finding the optimized control parameters over laser power or gate times

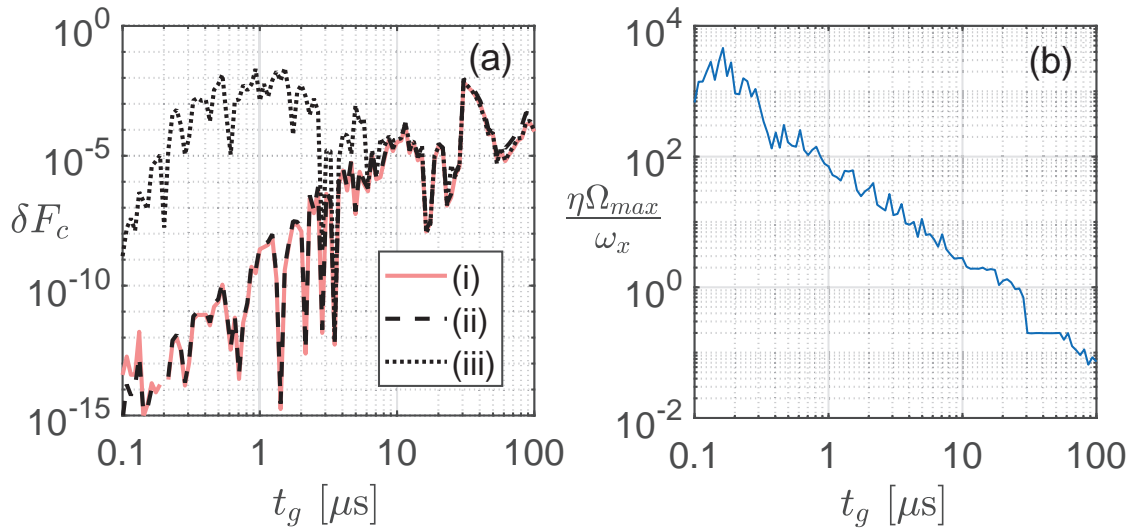


**Figure 3.** (a) The computational infidelities of a transverse-mode (the  $x$  or  $y$  directions) CPF gate using  $M = 7$  segment pulses for different gate times, using the pulse shapes obtained by considering a small array of  $N = 9$  and optimizing the fidelity over choices of  $\mu$  for a given  $t_g$  and  $T = 10T_D$  with  $T_D$  the Doppler temperature. Curve (i) corresponds to the original infidelity with the 3rd and 6th ions on the  $N = 9$  array. Curve (ii) corresponds to the infidelity of the transverse  $x$ -mode gate between the 628th and 631st ions (chosen randomly) on an  $N = 1795$  ion crystal. Curve (iii) corresponds to that of the transverse  $y$ -mode gate between the 624th and 627nd ions. In cases (ii) and (iii), we apply optical tweezers incident along the  $x$  direction on ions of index  $\{\dots, 625, 635, 645, \dots\}$  and create  $\omega_y^{\text{ot}} = 0.2\omega_x$  ( $\sim 2\pi \times 1$  MHz) trapping frequency in addition along the  $y$  direction on these ions. (b) The required intensity of the laser beam in terms of the maximal  $\eta\Omega$  of the pulse shape in (a). See text for the definitions for all quantities.

is however not the scope of this manuscript. We here focus on the effects on the gate fidelity when the system scales up according to the proposed scheme stabilised by optical tweezers.

In this section, we demonstrate an elementary quantum gate, control phase flip (CPF), on the  $i$ th and  $j$ th qubits by shining identical laser beams on them of engineered pulse shapes. An ideal CPF is described by  $U_{ij}^{\text{ideal}} = \exp\left(-i\frac{\pi}{4}\sigma_i^z\sigma_j^z\right)$  with  $\sigma_i^z$  the  $z$  component of the Pauli matrices for the  $i$ th qubit. Here we follow the pulse shaping scheme of quantum gate design [13, 28] but the push gate protocols [21, 23, 24, 26] may also apply without changing the main conclusion. This former scheme is based on the Sorensen-Molmer-Milburn gate protocol, where a pair of laser beams of slightly different colour are applied on the target qubits, resulting in state-dependent momentum kicks parallel to the wavevector difference  $\Delta\mathbf{k}$  of beat note frequency  $\mu$ . For quantum gates operating in the transverse (longitudinal) modes,  $\Delta\mathbf{k}$  needs to be along the  $x$  or  $y$  ( $z$ ) direction. In this work, we use transverse-mode gates for better protection from the noise [12]. The parameter  $\mu$  steers how motional modes are involved for it amounts to modulating the Rabi frequency  $\Omega^{(i,j)}(t) = \Omega_0(t) \sin \mu t$ , and hence the forces. As a result,

the gate dynamics can be given by the evolution operator

$$U(t) = \exp \left[ \sum_{i,k} \left( \alpha_i^k(t) a_k^\dagger + \alpha_i^{k*}(t) a_k \right) \sigma_i^z + i \sum_{i < j} \phi_{ij}(t) \sigma_i^z \sigma_j^z \right], \quad (2)$$

where  $\alpha_i^k(\tau) = \int_0^\tau dt \Omega_0(t) \eta_k G_{ik} e^{i\omega_k t}$  and  $\phi_{ij}(\tau) = 2 \int_0^\tau dt' \int_0^{t'} dt \sum_k \eta_k^2 G_{ik} G_{jk} \Omega_0(t) \Omega_0(t')$   $\sin \omega_k(t' - t)$  with the Lamb Dicke parameter  $\eta_k = |\Delta \mathbf{k}| \sqrt{\hbar/(m\omega_k)}$ .  $G_{ik}$  is the element of the canonical transformation matrix that diagonalizes  $A$ , i.e.,  $G^\top A G = A^D$  is diagonalised, corresponding to the  $i$ th ion and the  $k$ th eigenmode. We shape the pulse profile of gate duration  $t_g$  by chopping it into  $M$  equal time bins, and for each bin the amplitude of the Rabi frequency is set differently, i.e.,  $\Omega_0(t) = \Omega_m$  for  $(m-1)t_g/M < t \leq mt_g/M$ . The evolution operator (2) leads to a gate error, called the computational infidelity  $\delta F_c \equiv [6 - 2(\Gamma_i + \Gamma_j) - \Gamma_+ - \Gamma_-]/8$ , where  $\Gamma_i = \exp[-\sum_k |\alpha_i^k(t_g)|^2 \bar{\beta}_k/2]$  and  $\Gamma_\pm = \exp[-\sum_k |\alpha_i^k \pm \alpha_j^k|^2 \bar{\beta}_k/2]$  with  $\bar{\beta}_k = \coth[\hbar\omega_k/(k_B T)]$ .

The local motion consideration suggests that we take into account only a small subset of local ions. We thus model a quantum gate by considering a cell from an infinitely long ion crystal and freezing all the ions outside the cell. We then obtain the pulse shape from optimisation, and apply these parameters to the actual configuration of an ion crystal. For better estimation for the pulse shape, the cell of simulation must have a larger size than the target gate distance in order to take into account needed degrees of freedom. The more degrees are included, the more accurate of the gate simulation, along with the more computational load. For example, here we consider an  $N = 1795$  ion crystal stabilised by a series of optical tweezers shining on ions of index  $\{\dots, 625, 635, 645, \dots\}$  along the  $x$  direction. To obtain a pulse shape that implements a quantum gate between the 628th and 631st ions, we may turn to consider a gate between the 3rd and 6th ions within a 9-ion cell. The infidelity  $\delta F_c$  for varied gate times are plotted in Fig. 3(a). For the  $x$ -mode gates, the infidelity on a large array appears almost identical to the small array simulations, implying the validity of the local mode consideration. Note that optical tweezers play no role here since they have no effect on the motional spectrum of the  $x$  direction. But for the  $y$ -mode gates, increase in infidelity can be expected if optical tweezers alter the relevant mode spectrum. For comparison, we also look at the case with gate operation between the 624th and 627th ions (the 625th is tweezered). We find that the gate error increases significantly for  $t_g$  shorter than  $2 \mu\text{s}$ , as shown in Fig. 3(a). This is caused by intervention of the tweezered ion in between. For longer gate times ( $t_g \sim 2 \mu\text{s}$  and larger), surprisingly, the effect of tweezer frequency vanishes. Since gates of longer gate times more rely on interplay of the slower modes ( $\sim 100 \text{ kHz}$ ), insertion of optical tweezers of a few megahertz plays little role here. Also, in Fig. 3(b), we show the required laser power for various gate times in terms of the maximal Rabi frequency  $\eta\Omega_{\text{max}}$  of the pulse shape, and observe a power law  $\eta\Omega_{\text{max}} \sim t_g^{-1.53}$ . For gates longer than  $20 \mu\text{s}$ , the required  $\eta\Omega_{\text{max}}$  drops to about hundreds of kilohertz, a typical range of laser power currently available.

In addition to the computational infidelity  $\delta F_c$  originating from imperfect disentangling between qubits and motion at the computing stage, there are other major



sources of error associated with the temperature. The first one is owing to breakdown of Lamb-Dicke approximation when the thermal fluctuations in ions' displacement become non-negligible compared to the wavelength of the laser field. This error of a transverse-mode gate has been shown to be  $\delta F_{\text{LD}}^{\xi=x,y} \approx \pi^2 \eta_\xi^4 (\bar{n}_\xi^2 + \bar{n}_\xi + 1/8)$  [12], and  $\bar{n}_\xi$  is the mean phonon number of the  $\xi$  mode. For large  $\bar{n}_\xi$ , this form can be recast as  $\delta F_{\text{LD}}^\xi \approx \pi^2 (\Delta k)^4 (\delta x_{\text{th}}^\xi)^2$ , where  $\delta x_{\text{th}}^\xi$  is the mean position fluctuation of a motional thermal state. The second source of error comes from the high-order contribution beyond the harmonic approximation for normal modes. This error can be characterised by  $\delta F_a^{\xi=x,y,z} \approx (\delta x_{\text{th}}^\xi/d_0)^2$  [13]. The third one is associated with the single qubit addressability. As an ion is illuminated by a laser beam of Gaussian profile  $\Omega \sim \exp[-(z - z_0)^2/w^2]$ , where  $z_0$  is the equilibrium position of the ion and  $w$  is the beam size, it sees spatially dependent field intensity due to its longitudinal motion. This non-uniformity of the driving field introduces an infidelity  $\delta F_b^z = (\pi^2/4)(\delta z_{\text{th}}/w)^4$ . In the following section, we will see how these infidelities are taken care of through cooling.

#### 4. Cooling

A large array of ions is subjected to serious heating and needs to be continuously cooled not just for stabilising the array structure but also sustaining the quantum coherence. When some ion qubits have carried quantum information and cannot be directly cooled, one can still cool their neighbours (coolant ions) to help remove the heat through momentum exchange. Such a sympathetic cooling scheme has been commonly used and studied [31, 32, 33, 34, 35]. In this section, we discuss the performance of this scheme in the presence of optical tweezers.

The mathematical model for sympathetic cooling has been discussed in [35], where every ion is coupled to its own thermal bath but linked with each other by Coulomb interaction. The Heisenberg-Langevin's equation for this system is given by

$$\begin{aligned} \dot{x}_i^\xi &= p_i^\xi \\ \dot{p}_i^\xi &= - \sum_j A_{ij}^\xi x_j^\xi - \gamma_i^\xi p_i^\xi + \sqrt{2\gamma_i^\xi} \eta_i^\xi, \end{aligned} \quad (3)$$

where  $x_i^\xi$  and  $p_i^\xi$  are the  $i$ th ion's coordinate and momentum operators along the  $\xi$  direction in units of  $d_0$  and  $m\omega_0 d_0$ , respectively,  $\gamma_i^\xi$  is the damping rate characterising the coupling between the ion and its environment, and  $\eta_i^\xi$  corresponds to random kicks owing to the baths. For Markov baths, we take  $\langle \eta_i^\xi(t) \eta_j^\xi(t') \rangle = \delta_{ij} \delta(t - t') \sum_k \tilde{\omega}_k G_{ik}^2 (\bar{n}_k^{\xi,B}(\tilde{T}_i) + 1/2)$ , where the mean phonon number of the thermal distribution  $\bar{n}_k^{\xi,B}(\tilde{T}) = [\exp(\tilde{\omega}_k/\tilde{T}) - 1]^{-1}$  with  $\tilde{\omega}_k = \omega_k/\omega_0$  and  $\tilde{T} = k_B T/(\hbar\omega_0)$ . For coolant ions, we assume that their bath temperature is the Doppler temperature  $T_D$ , and the associated damping rate  $\gamma_i = 0.01$  corresponds to a typical retardation coefficient given by the Doppler cooling. For rest of the ions, we model background heating by setting  $\gamma_i^\xi \tilde{T}_i = 10^{-4}$ , which amounts to a heating rate of about 60 phonons per second per ion for the frequency level  $\sim \omega_0$ . To study the worse case scenarios, we take  $\tilde{T}_i \rightarrow \infty$

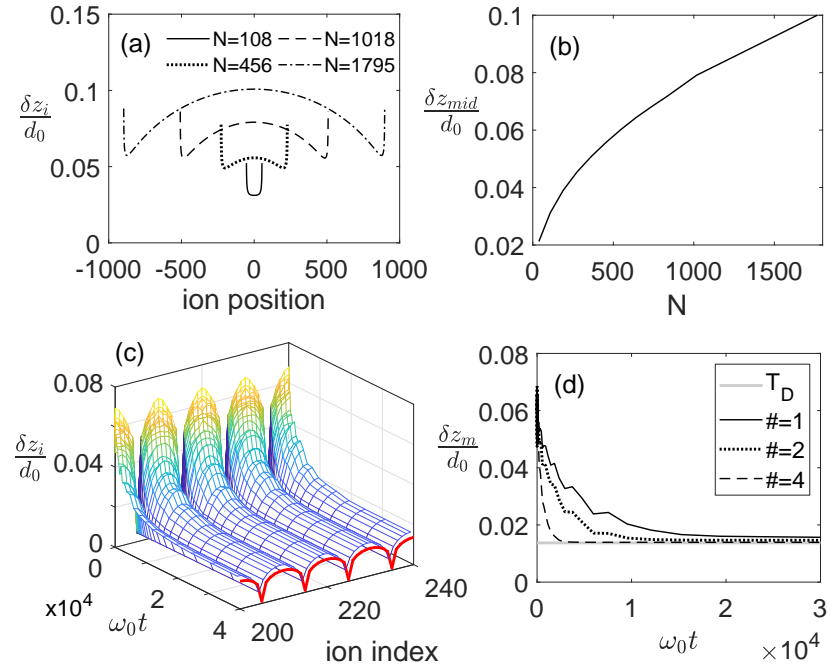


**Figure 4.** (a) The longitudinal position fluctuation (PF) of ion arrays of different length without optical tweezers. (b) The longitudinal PF  $\delta z_{mid}$  corresponding to the middle of the ion crystal as a function of the system size  $N$  without optical tweezers. Note that the curve can be fitted by  $\delta z_{mid}/d_0 = 4.3 \times 10^{-3} N^{0.42}$ , which reaches  $1 \mu\text{m}$  when  $N \sim 1800$ . (c) Cooling dynamics in terms of  $\delta z_i$  of the 200th to 240th ions on an  $N = 1018$  ion crystal with optical tweezers and sympathetic cooling. Here, optical tweezers are applied on ions of index  $\{..., 205, 215, 225, ...\}$ ; Doppler cooling beams are applied on ions of index  $\{..., 206, 216, 226, ...\}$ . For reference, the red curve shows the PF profile at  $T = T_D$ . (d) The temporal relaxation of the longitudinal PF of the 240th ion,  $\delta z_m$ , corresponding to the middle one within the cell (locally maximally displaced). The solid curve labeled by  $\# = 1$  corresponds to the case in (c), with a single Doppler cooling beam for each cell. The dotted curve by  $\# = 2$  and the dashed curve by  $\# = 4$  correspond to the cases with two and four Doppler beams for each cell, respectively, applied on the adjacent ions of both sides of each tweezered ion equally. By fitting to an exponential profile ( $\delta z_m = ae^{-t/\tau_R} + \delta z_s$ ), we have the relaxation times  $\tau_R^z$  of  $4900\omega_0^{-1}$ ,  $2590\omega_0^{-1}$ , and  $677\omega_0^{-1}$  and  $\delta z_s = 0.016d_0$ ,  $0.015d_0$ , and  $0.014d_0$ , respectively. The horizontal reference line corresponds to the middle ion's longitudinal PF ( $= 0.014d_0$ ) at  $T = T_D$ .

with  $\gamma_i^\xi = 10^{-4}/\tilde{T}_i$  and look at the resultant position fluctuation (PF) defined by  $\delta x_i^\xi = [\langle x_i^2 \rangle - \langle x_i \rangle^2]^{1/2}$  of the  $i$ th ion.

Figure 4(a) shows the distribution of the longitudinal PF for various array sizes without optical tweezers. Neglecting those ions on the array edges, the greatest one  $\delta z_{mid}$  occur at the centre of the array. We find the scaling relation  $\delta z_{mid}/d_0 = 4.3 \times 10^{-3} N^{0.42}$  at  $T_D$  as shown in Fig. 4(b). Even when the whole system is Doppler cooled,  $\delta z_{mid}$  becomes larger than 10% ( $1 \mu\text{m}$ ) of the ion spacing ( $10 \mu\text{m}$ ) for  $N \sim 1800$  and larger. This not only results in very large  $\delta F_a^z$ ,  $\delta F_b^z$  (approximately or larger than  $10^{-2}$ ) but also makes the whole array unstable. Now we turn to the optical tweezer assisted configuration.

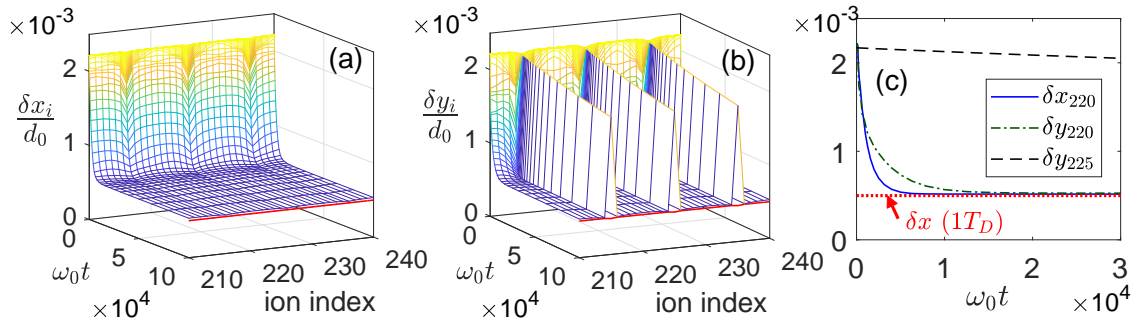


**Figure 5.** Transverse cooling dynamics in terms of (a)  $\delta x_i$  and (b)  $\delta y_i$  for the 210th to 240th ions on an  $N = 1018$  ion crystal with optical tweezers (along the  $x$  direction) and sympathetic cooling on the  $x$  and  $y$  modes, respectively. The arrangement of optical tweezers is the same as Fig. 4(c). (c) The temporal profiles of the transverse PFs of the 220th ion,  $\delta x_m$  and  $\delta y_m$ , corresponding to the middle one within the cell. By fitting to an exponential profile ( $\delta x_m^\xi = ae^{-t/\tau_R^\xi} + \delta x_s^\xi$ ), we have the relaxation times  $\tau_R^x = 113\omega_0^{-1}$ ,  $\delta x_s = 5.1 \times 10^{-4}d_0$  for the  $x$  modes, and  $\tau_R^y = 302\omega_0^{-1}$ ,  $\delta y_s = 5.3 \times 10^{-4}d_0$  for the  $y$  modes. For comparison, the profile of the 225th (tweezered) ion is plotted with  $\tau_R^y = 1.25 \times 10^4\omega_0^{-1}$  and  $\delta y_s = 1.6 \times 10^{-3}d_0$ . The horizontal reference line corresponds to the middle ion's PF ( $= 5.1 \times 10^{-4}d_0$ ) at  $T = T_D$ .

For demonstration, we place optical tweezers on the ion array with a spatial period  $P = 10$ , and simultaneously Doppler cool the neighbouring ions next to the tweezered ones. Fig. 4(c) shows the cooling dynamics of the array starting from  $T = 20T_D$  at  $t = 0$ , where we observe that the overall  $\delta z_i$  goes down almost exponentially, and asymptotically approaches to a steady-state value. Specifically, we look at the middle ion (220th) within a cell defined by two tweezered ones (215th and 225th), and plot its PF relaxation in Fig. 4(d). From this curve, we extract a relaxation time  $\tau_R^z$  by fitting to an exponential profile. Our calculation shows that  $\tau_R^z$  is on the order of a few milliseconds if one ion is Doppler cooled within this cell. Increasing the number of coolant ions shortens  $\tau_R$  down to sub-milliseconds. It can be also shown that the steady state is very close to the Doppler temperature with PF suppressed down to about 2% of  $d_0$ , resulting in much smaller  $\delta F_a^z \sim 4 \times 10^{-4}$  and  $\delta F_b^z \sim 10^{-5}$ .

On the other hand, since the transverse frequency is on the order of megahertz, the associated PFs  $\delta x_i$  or  $\delta y_i$  are about one order of magnitude smaller than  $\delta z_i$ . Note that only the  $y$ -mode fluctuations are affected by the optical tweezers applied along the  $x$  direction. These fluctuations contribute majorly to the gate fidelity  $\delta F_{LD}^{x,y}$  and  $\delta F_a^{x,y}$ . Given  $\delta x_{th}^\xi/d_0 = 5.1 \times 10^{-4}$  at  $T_D$ ,  $\delta F_{LD}^{x,y} = 7.0 \times 10^{-4}$  and  $\delta F_a^{x,y} \sim 10^{-7}$ . In Fig. 5, we show the relaxation dynamics of  $\delta x_i$  and  $\delta y_i$  under the similar arrangement of Fig. 4(c). The steady-state PF is almost identical to that given at  $T_D$ , resulting in similar infidelities. On the other hand, we find that the  $x$ -mode PF presents much faster relaxation without effects of optical tweezers compared to the  $y$ -mode PF. This contradicts to the intuition we hold for the longitudinal mode, where the optical tweezers play a positive role that improves cooling efficiency. Due to frequency mismatch of the local tweezers to the neighbouring ions, the heat tends to be trapped on the tweezered

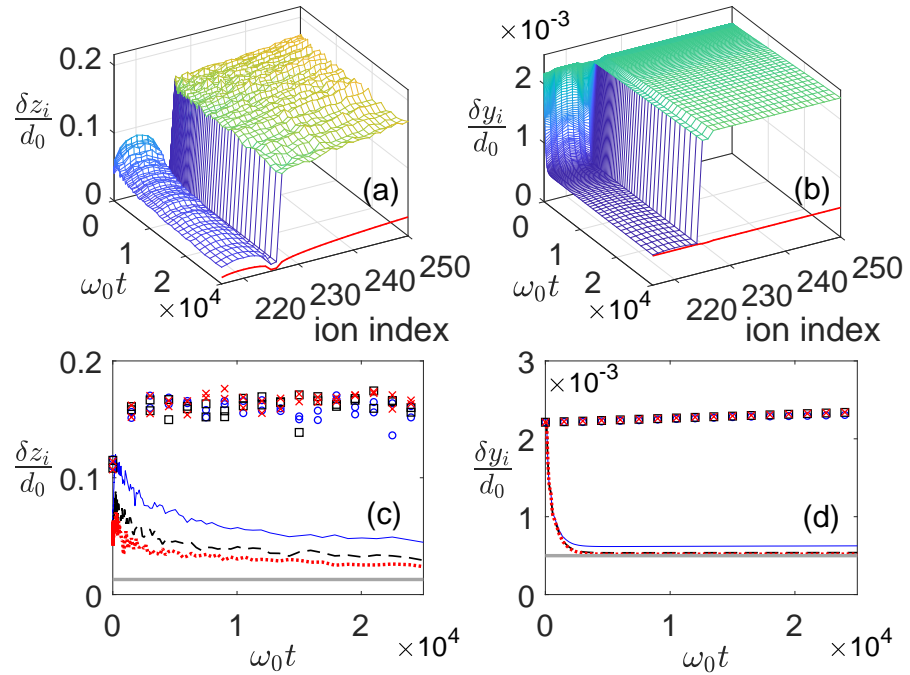


**Figure 6.** Cooling dynamics of (a) longitudinal and (b) transverse PFs,  $\delta z_i$  and  $\delta y_i$ , respectively, on an  $N = 1018$  ion crystal. Optical tweezers are applied on the ions of index  $\{214, 215, 225, 226\}$  while the Doppler cooling is performed on the ions of index  $\{216, 217, 223, 224\}$ . For reference, the supposed PF profiles at the Doppler temperature are plotted in red. We can see that the temperature in terms of PF within the cell can be made much lower than that outside the cell and to the Doppler one. Also, relaxation curves of the (c) longitudinal and (d) transverse PFs, respectively, of the 220th ion (the middle one in the cell) are plotted. The solid (blue), dashed (black), and dotted (red) curves correspond to cases with the walls of the cell formed by one, two, and three tweezered ions, respectively, on each side. When fitted to an exponential profile  $\delta x^\xi = ae^{-t/\tau_R^\xi} + \delta x_s^\xi$ , we find  $\tau_R^z = 3.9 \times 10^4 \omega_0^{-1}$ ,  $2.4 \times 10^4 \omega_0^{-1}$ ,  $1.7 \times 10^4 \omega_0^{-1}$  and  $\delta z_s = 0.031d_0$ ,  $0.025d_0$ ,  $0.021d_0$ , respectively, and  $\tau_R^y = 658 \omega_0^{-1}$ ,  $698 \omega_0^{-1}$ ,  $709 \omega_0^{-1}$  and  $\delta y_s = 6.1 \times 10^{-4}d_0$ ,  $5.3 \times 10^{-4}d_0$ ,  $5.2 \times 10^{-4}d_0$ , respectively. For comparison, the horizontal reference lines correspond to the middle ion's longitudinal and transverse PFs at  $T = T_D$ . The PFs corresponding to the 190th and 250th ions (30 sites away from the cell center) are also plotted, showing the heating effect outside the cell.

sites, exhibiting higher PFs and slower relaxation as shown in Fig. 5(b).

## 5. Local trap and cooling

We have learned from previous analysis that optical tweezers effectively play a role to serve as separators that partitions the whole ion crystal into sub-arrays. A cell can be defined given two or two groups of tweezered ions on both sides containing a sub-array. And the thickness of a cell wall can be thought as the number of tweezered ions placed next to each other. Intuitively speaking, a cell can be made less coupled to the rest of the ion crystal in terms of momentum exchange by increasing the wall thickness.

Therefore, it is possible to cool a cell that has its own temperature within a timescale of interest. If this is the case, one can implement a faithful quantum gate within a locally cooled cell without spending resources on cooling irrelevant ions. In this section, we investigate the local dynamics of sympathetic cooling on a chosen cell while other parts of the array may be gradually heated by thermal noises.

Here we take an exemplary case by considering a large ion array of  $N = 1018$ , on which we choose a cell that contains ions of index  $\{216, \dots, 224\}$ . Next to the edge ions, we shine optical tweezer beams to form two walls of the same thickness for the cell. To sympathetically cool those ions within, we apply Doppler cooling on the edge ions of index  $\{216, 217, 223, 224\}$ , and look at the local dynamics of PF. Fig. 6(a) and (b) show the profiles of  $\delta z_i$  and  $\delta y_i$ , respectively, of the 216th  $\sim$  250th ions, where we set the initial temperature to be  $20T_D$ . As expected, we find that PFs within the cell decrease with time nearly exponentially and approach to a steady-state distribution, which is found to be slightly larger than that at  $T_D$  due to the presence of background heating. In the case where the wall thickness is two on both sides, we have the cooled (steady-state) PF  $\delta z_s \approx 0.025d_0$  with relaxation time  $\tau_R^z \approx 26$  ms, and  $\delta y_s \approx 5.3 \times 10^{-4}d_0$  with  $\tau_R^y \approx 0.78$  ms for the longitudinal and transverse modes, respectively, thus keeping all the largest gate infidelities discussed in the previous sections on the order of  $10^{-4}$ .

The steady-state fluctuation profile of the cell can be made arbitrarily close to the ideally Doppler cooled case by increasing the number of coolant ions and thickening the cell walls, as shown in Fig. 6(c) and (d) for longitudinal and transverse directions, respectively. Heating can be generally observed for ions outside the cell. For the longitudinal motion, the fluctuations appear to be slightly suppressed for ions closer to the cell. But for the transverse one, the fluctuation profile tends to be more independent of locations. This is because the longitudinal modes are soft ones with longer oscillation periods ( $\sim \omega_L^{-1}$ ), allowing momentum exchange (characterised by  $\omega_0^{-1}$ ) to take place between distant ions over the walls. This is generally not the case for transverse modes ( $\sim \omega_{x,y}^{-1}$ ), whose periods are too short to support exchange momentum between distant ones.

## 6. Conclusion

To sum up, we have proposed an ion crystal architecture stabilised by optical tweezers. In a traditional RF ion trap, a large array usually has collective modes of vanishing frequencies in the longitudinal direction and hence divergent motional excitation given any finite temperature, making its structure vulnerable. Though typically the Coulomb interaction is much stronger than dipole forces given by optical tweezers, the relevant motional frequency scale is determined by the next-order contribution, the residual Coulomb interaction, characterised by  $\omega_0$ , which is about hundreds of kilohertz for ion separation about  $10 \mu\text{m}$ . Thus, application of optical tweezers is able to alter the longitudinal motional spectrum and lifts the frequencies of the ground modes by appropriately arranging the optical tweezers. Further, it has been shown that ions

illuminated by optical tweezers can be seen effectively pinned in space by comparing the motional spectra. Cells can be thus defined by being sandwiched by tweezered ions, introducing the convenience to look at localised motion associated with these cells.

For a large-scale computing, making operations depending on local degrees of freedom is very important. This allows parallel processing and pipelined task management. We have also shown faithful quantum logic gates based on transverse modes for two free (not tweezered) ions within a cell. It should be emphasized that these gates are implemented using the controlling parameters obtained in a small array simulation. This implies that these parameters have translation symmetry along the ion crystal, that is, universal to anywhere of implementation given the same gate distance. The presence of optical tweezers, depending on the incident direction, may alter the motional spectrum that transverse gates are based on. We have shown that the gate error can still be kept lower than  $10^{-5}$  unless optical tweezers intervene the ions between the target qubits.

In addition to the computational error associated with the gate design, we have also investigated other major sources of imperfection, such as breakdown of the Lamb-Dicke approximation, anharmonicity, and a non-uniform beam profile, which require cooling to reduce the longitudinal and transverse PFs for insuring the gate fidelity. For this purpose, we have examined the sympathetic cooling dynamics in the presence of optical tweezers. The advantage of applying optical tweezers is apparent: with regular arrangement of tweezers along the system, the overall PFs can be greatly suppressed compared to the cases without them, where the PFs basically diverge as the system size increases. We can thus maintain the whole system close to the Doppler temperature with thermal effects contributing only about  $10^{-4}$  of gate errors. Finally, we have looked into the locality of motion for a cell by adding more tweezered ions to increase the wall thickness. Note that such locality is a remarkable feature because trapped ions are usually collectively coupled so that, without optical tweezers, local manipulations tend to cause long-range interferences. For the concern of parallel computing, these interferences are unwanted effects but can now be eliminated with the help of optical tweezers. We have shown that a cell can be cooled almost independently from other parts of the system, thus suggesting a more economical way to spending resources for cooling issues. Further, we expect that our proposed scheme also interests communities of quantum simulation of cavity quantum electrodynamics for the resemblance between a cell defined by tweezers for phonons and a real cavity for photons, and quantum thermodynamics for the analogue of heat transfer.

## Acknowledgments

We thank the support from MOST of Taiwan under Grant No. 105-2112-M-002-015-MY3 and National Taiwan University under Grant No. NTU-106R891708. GDL thanks M.-S. Chang for valuable discussion and feedback.

- [1] Ballance C J, Harty T P, Linke N M, Sepiol M A and Lucas D M 2016 High-fidelity quantum logic gates using trapped-ion hyperfine qubits *Phys. Rev. Lett.* **117** 060504
- [2] Gaebler J P, Tan T R, Lin Y, Wan Y, Bowler R, Keith A C, Glancy S, Coakley K, Knill E, Leibfried D and Wineland D J 2016 High-fidelity universal gate set for 9 Be<sup>+</sup> ion qubits *Phys. Rev. Lett.* **117** 060505
- [3] Schfer V M, Ballance C J, Thirumalai K, Stephenson L J, Ballance T G, Steane A M and Lucas D M 2018 Fast quantum logic gates with trapped-ion qubits *Nature* **555** 75–78
- [4] Monz T, Schindler P, Barreiro J T, Chwalla M, Nigg D, Coish W A, Harlander M, Hensel W, Hennrich M and Blatt R 2011 14-Qubit entanglement: creation and coherence *Phys. Rev. Lett.* **106** 130506
- [5] Bohnet J G, Sawyer B C, Britton J W, Wall M L, Rey A M, Foss-Feig M, Bollinger J J 2016 Quantum spin dynamics and entanglement generation with hundreds of trapped ions *Science* **352** 1297–1301
- [6] Wright K, Beck K M, Debnath S, Amini J M, Nam Y, Grzesiak N, Chen J-S, Piseni N C, Chmielewski M, Collins C, Hudek K M, Mizrahi J, Wong-Campos J D, Allen S, Apisdorf J, Solomon P, Williams M, Ducore A M, Blinov A, Kreikemeier S M, Chaplin V, Keesan M, Monroe C, Kim J 2019 Benchmarking an 11-qubit quantum computer arXiv:1903.08181
- [7] Richerme P, Gong Z-X, Lee A, Senko C, Smith J, Foss-Feig M, Michalakakis S, Gorshkov A V and Monroe C 2014 Non-local propagation of correlations in quantum systems with long-range interactions *Nature* **511** 198–201
- [8] Jurcevic P, Lanyon B P, Hauke P, Hempel C, Zoller P, Blatt R and Roos C F 2014 Quasiparticle engineering and entanglement propagation in a quantum many-body system *Nature* **511** 202
- [9] Senko C, Smith J, Richerme P, Lee A, Campbell W C and Monroe C 2014 Coherent imaging spectroscopy of a quantum many-body spin system *Science* **345**, 430–433
- [10] Sørensen A and Mølmer K 1999 Quantum computation with ions in thermal motion *Phys. Rev. Lett.* **82** 1971
- [11] Milburn G J, Schneider S and James D F V 2000 Ion Trap Quantum computing with warm ions *Fortschr. Physik* **48** 801
- [12] Zhu S L, Monroe C, Duan L M 2006 Trapped ion quantum computation with transverse phonon modes *Phys. Rev. Lett.* **97** 050505
- [13] Lin G-D, Zhu S-L, Islam R, Kim K, Chang M-S, Korenblit S, Monroe C and Duan L-M 2009 Large-scale quantum computation in an anharmonic linear ion trap *EPL* **86** 60004
- [14] Kielpinski D, Monroe C and Wineland D J 2002 Architecture for a large-scale ion-trap quantum computer *Nature* **417** 709–711
- [15] Blakestad R B, Ospelkaus C, VanDevender A P, Wesenberg J H, Biercuk M J, Leibfried D and Wineland D J 2011 Near-ground-state transport of trapped-ion qubits through a multidimensional array *Phys. Rev. A* **84** 032314
- [16] Moehring D L, Highstrete C, Stick D, Fortier K M, Haltli R, Tigges C and Blain M G 2011 Design, fabrication and experimental demonstration of junction surface ion traps *New J. Phys.* **13** 075018
- [17] Monroe C and Kim J 2013 Scaling the ion trap quantum processor *Science* **339** 1164–1169
- [18] Duan L-M, Blinov B B, Moehring D L and Monroe C 2004 Scalable trapped ion quantum computation with a probabilistic ion-photon mapping *Quantum Information and Computation* **4** 165–173
- [19] Duan L-M and Monroe C 2010 Quantum networks with trapped ions *Rev. Mod. Phys.* **82** 1209
- [20] Cirac J I and Zoller P 2000 A scalable quantum computer with ions in an array of microtraps *Nature* **404** 579–581
- [21] Ratcliffe A K, Taylor R L and Hope J J 2018 Scaling trapped ion quantum computers using fast gates and microtraps *Phys. Rev. Lett.* **120** 220501
- [22] Wineland D J, Monroe C, Itano W M, Leibfried D, King B E and Meekhof D M 1998 Experimental issues in coherent quantum-state manipulation of trapped atomic ions *J. Res. NIST* **103** 259

- [23] Garcia-Ripoll J J, Zoller P, and Cirac J I 2003 Speed optimized two-qubit gates with laser coherent control techniques for ion trap quantum computing *Phys. Rev. Lett.* **91** 157901
- [24] Duan L-M 2004 Scaling ion trap quantum computation through fast quantum gates *Phys. Rev. Lett.* **93** 100502
- [25] Steane A M, Imreh G, Home J P and Leibfried D 2014 Pulsed force sequences for fast phase-insensitive quantum gates in trapped ions *New J. Phys.* **16** 053049
- [26] Bentley C D B, Carvalho A R R and Hope J J 2015 Trapped ion scaling with pulsed fast gates *New J. Phys.* **17** 103025
- [27] Garcia-Ripoll J J, Zoller P and Cirac J I 2005 Coherent control of trapped ions using off-resonant lasers *Phys. Rev. A* **71** 062309
- [28] Zhu S-L, Monroe C and Duan L-M 2006 Arbitrary-speed quantum gates within large ion crystals through minimum control of laser beams *EPL* **73** 485–491
- [29] Palmero M, Martinez-Garaot S, Leibfried D, Wineland D J and Muga J G 2017 Fast phase gates with trapped ions *Phys. Rev. A* **95** 022328
- [30] Herold C D, Fallek S D, Merrill J T, Meier A M, Brown K R, Volin C E and Amini J M 2016 Universal control of ion qubits in a scalable microfabricated planar trap *New J. Phys.* **18** 023048
- [31] Kielpinski D, King B E, Myatt C J, Sackett C A, Turchette Q A, Itano W M, Monroe C, Wineland D J and Zurek W H 2000 Sympathetic cooling of trapped ions for quantum logic *Phys. Rev. A* **61** 032310
- [32] Barrett M D, DeMarco B, Schaetz T, Meyer V, Leibfried D, Britton J, Chiaverini J, Itano W M, Jelenković B, Jost J D, Langer C, Rosenband T and Wineland D J 2003 Sympathetic cooling of  $^9\text{Be}^+$  and  $^{24}\text{Mg}^+$  for quantum logic *Phys. Rev. A* **68** 042302
- [33] Home J P, McDonnell M J, Szwer D J, Keitch B C, Lucas D M, Stacey D N and Steane A M 2009 Memory coherence of a sympathetically cooled trapped-ion qubit *Phys. Rev. A* **79** 050305(R)
- [34] Brown K R, Ospelkaus C, Colombe Y, Wilson A C, Leibfried D and Wineland D J 2011 Coupled quantized mechanical oscillators *Nature* **471** 196–199
- [35] Lin G-D and Duan L-M 2016 Sympathetic cooling in a large ion crystal *Quantum information processing* **15** 5299-5313